Eclética Química Journal

Original article

revista.iq.unesp.br

| Vol. 47 | special issue 1 | 2022 |

Influence of Cu-doped TiO_2 on its structural and photocatalytic properties

Vinícius Teodoro[1], Elson Longo[1], Maria Aparecida Zaghete[2], Leinig Antonio Perazolli[2+]

1. Federal University of Sao Carlos, Center for the Development of Functional Materials, São Carlos, Brazil.
2. São Paulo State University, Institute of Chemistry, Araraquara, Brazil.

+Corresponding author: Leinig Antonio Perazolli, **Phone:** +551633019711, **Email address:** leinig.perazolli@unesp.br

ARTICLE INFO

Article history:
Received: July 26, 2021
Accepted: December 09, 2021
Published: April 11, 2022

Section Editors: Elson Longo and Juan Manuel Andrés Bort

Keywords:
1. photocatalysis
2. titanium dioxide
3. doping
4. UV light

ABSTRACT: Due to the potential of heterogeneous photocatalysis for wastewater treatment, the researches concerning the improvement materials modifications for its photocatalytic activity have been widely increased. One of the most employed methods is the metal doping into semiconductors. Herewith, we demonstrated the influence of Cu doping into TiO_2 in its photocatalytic properties. The powder samples with 0.0 to 0.7% mol were obtained by the Pechini method and characterized by XRD, micro-Raman spectroscopy, FE-SEM, and photoluminescence spectroscopy. The Cu insertion into TiO_2 structure induced the stabilization of anatase phase, increasing its content in the samples in relation to the bare TiO_2. The PL results indicated that a decrease in the PL emission intensity and a shift of the emission band to the blue region. The photocatalytic activity for rhodamine B degradation under UV light irradiation indicated that the Cu-doping into TiO_2 led to an enhancement of the photocatalytic activity compared to the bare one.

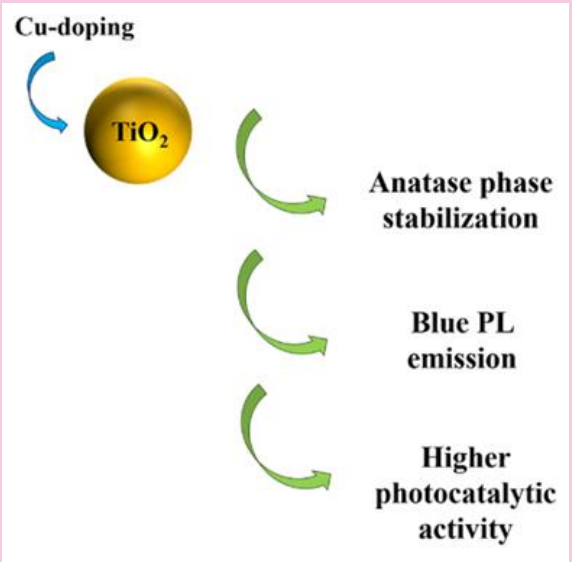

ISSN: 1678-4618
DOI: 10.26850/1678-4618eqj.v47.1SI.2022.p130-140

1. Introduction

Due to increasing of industrial disposal and domestic effluents on recent years, such as wastewater, it has become necessary an effective treatment alternative to improve the environment quality. Among several methods, heterogeneous photocatalysis has been studied as an alternative to such problem due to its potential degradation of organic compounds, allowing water and air purification (Fujishima *et al.*, 2000; Galindo *et al.*, 2000; Gaya and Abdullah, 2008; Qourzal *et al.*, 2005; Silva *et al.*, 2020). Therefore, the search for materials with high photocatalytic activity and potential to solar applications has been the main target of researches.

The titanium dioxide (TiO_2) is odorless, has high acid resistance and act as a UV absorbent. The most important functions are as a widely used pigment, solar protection and photocatalyst for organic compounds. Titanium dioxide also has been used as a bleaching and opacifying agent in porcelain enamels, giving them brightness, hardness, and acid resistance. TiO_2 is one of the most widely investigated for photocatalytic applications due to its high oxidizing ability for organic pollutants, low cost, photostability, nontoxicity and chemical stability (Dashora *et al.*, 2014; Nakata and Fujishima, 2012; S. Wang *et al.*, 2014). Numerous studies were published on the photocatalytic TiO_2 applications for the decomposition of organic compounds due to the ability of TiO_2 to oxidize organic and inorganic substances in water and air through redox processes (S. Wang *et al.*, 2014), TiO_2 only absorbs ultraviolet (UV) light of broad solar spectrum due to its large bandgap energy ($\lambda < 388$ nm), which was comprised of only 4% of the entire solar spectrum (Dashora *et al.*, 2014; H. Wang *et al.*, 2015).

Furthermore, the high recombination rate of electron/hole pair (e^-/h^+) within the semiconductor is the main problem for the photocatalytic performance of the semiconductor, since it disables the photoexcited electron and the hole for redox reactions (Rashad *et al.*, 2014; Li Zhang *et al.*, 2014).

In order to improve the photocatalytic performance of TiO_2, modifications in its structure have been investigated, such as doping with metals ions (Li *et al.*, 2016; Sanchez-Dominguez *et al.*, 2015; Q. Wang *et al.*, 2017; Xiao *et al.*, 2016). The substitution of a Ti^{4+} by another transition metal ion promotes changes in the coordination parameters, thus altering the electronic and optical properties, resulting in attractive characteristics for photocatalytic applications (Chen *et al.*, 2018a; Vargas Hernández *et al.*, 2017). Several advantages concerning doping on TiO_2 have been reported, such as increase of specific surface area, light absorption capacity, and charge transfer rate on particle surface, and band gap energy reduction (Carp *et al.*, 2004; G. Liu *et al.*, 2010). The Cu doping on TiO_2 has shown improvement and desirable results for antibacterial applications (Lan Zhang *et al.*, 2016) and for high-rate capability for lithium-ion batteries (Y. Zhang *et al.*, 2016), possibly making it an attractive dopant metal for photocatalytic applications.

In this work, we report the influence of Cu-doped on TiO_2 powders prepared by the Pechini method and its effects on structural and photocatalytic properties for degradation of rhodamine B dye (RhB) under UV light irradiation. These obtained powders were characterized using XRD, MR spectroscopy, FE-SEM, and PL spectroscopy.

2. Experimental

2.1 Synthesis

All chemical reagents were of analytical grade and used without further treatment. The powders were obtained by the Pechini method, which were used titanium isopropoxide (purity 95%, Alfa Aesar), citric acid (purity 99.5%, Synth) and ethylene glycol (purity 99%, Synth) in a ratio of 1:4:16 moles, respectively. Ethylene glycol was heated to 70 °C and then, titanium isopropoxide was added and stirred for 20 min. Citric acid was added to the mixture and this was stirred for 2 h at 90 °C. The polymeric solution was standardized by gravimetry method in order to define content of TiO_2 generated per gram of solution. For the Cu-doped TiO_2 samples, $Cu(NO_3)_2.3H_2O$ was added to the polymeric solution in stoichiometric contents to obtain 0.3, 0.5 and 0.7 at.% of Cu related to Ti, which the samples were denominated as CTO-0, CTO-0.3, CTO-0.5, and CTO-0.7, respectively. The polymeric solutions were annealed at 380 °C for 4 h to form the root solid, and then 400 °C for 10 h to eliminate organic compounds. All concentrations of Cu-doped and bare TiO_2 samples were annealed 600 °C for 4 h.

2.2 Characterizations

The morphological, structural and optical properties of samples were characterized by field-emission scanning electron microscopy (FE-SEM, JEOL 7500F), X-ray diffraction (XRD, Rigaku-Rotalex Dmax/2500 PC) with Cu Kα radiation, micro-Raman spectroscopy (MR, Horiba Jobin Yvon LabRAM iHR550) with a laser wavelength of 514 nm. The optical spectroscopy in UV-Vis on diffuse reflectance mode was performed in a

Eclética Química Journal, vol. 47, special issue 1, 2022, 130-140
ISSN: 1678-4618
DOI: 10.26850/1678-4618eqj.v47.1SI.2022.p130-140

Perkin Elmer spectrophotometer (Lambda 1050 UV/Vis/NIR). The photoluminescence spectroscopy (PL) was performed at room temperature under air atmosphere using a Monospec 27 monochromator (Thermal Jarrel Ash, USA) coupled to an R955 photomultiplier (Hamamatsu Photonics, Japan). A krypton ion laser (Coherent, Innova 200) with wavelength of 350 nm, with maximum output power maintained at 500 mW and maximum power of 14 mW on the sample due to the passage through an optical chopper. The surface area was measured using Brunauer-Emmett-Teller (BET) methods and Micromeritics ASAP 2010 equipment.

2.3 Photocatalytic experiments

The photocatalytic performance of all samples was carried out in a Philips Ouro reactor, which was fitted with a quartz tube and an inner UV germicide lamp (λ = 254 nm, 11 W, Osram, Puritec HNS 2G7). The reactor was 9.4 cm of inside diameter and 17.2 cm of height, the quartz tube was 4.1 cm of the inside diameter and 22 cm of height which was sustained by a support. The UV germicide lamp was inside the quartz tube and has dimensions of 1.2 × 2.6 × 19 cm. The experiments were conducted with 700 mL of rhodamine B dye (RhB) solutions (10^{-5} mol L^{-1}), 70 mg of catalyst and under constant agitation and pumping air to saturation of O_2 dissolved. At certain times, aliquots were withdrawal and centrifuged for absorbance measurements in a Perkin Elmer spectrophotometer (Lambda 1050 UV/Vis/NIR).

3. Results and discussion

Figure 1a shows the XRD patterns of Cu-doped and bare TiO_2 samples obtained by the Pechini method. For all samples, the anatase and rutile phases of TiO_2 were observed, according to the Inorganic Crystal Structure Database (ICSD) code 9852 and code 9161, respectively. The presence of rutile phase is due to its thermodynamic stability in synthesis temperature from 600 °C (Hu *et al.*, 2003; Zhu *et al.*, 2015). No peaks related to any Cu-related phase were observed, indicating the incorporation of Cu^{2+} into the TiO_2 lattice as dopant.

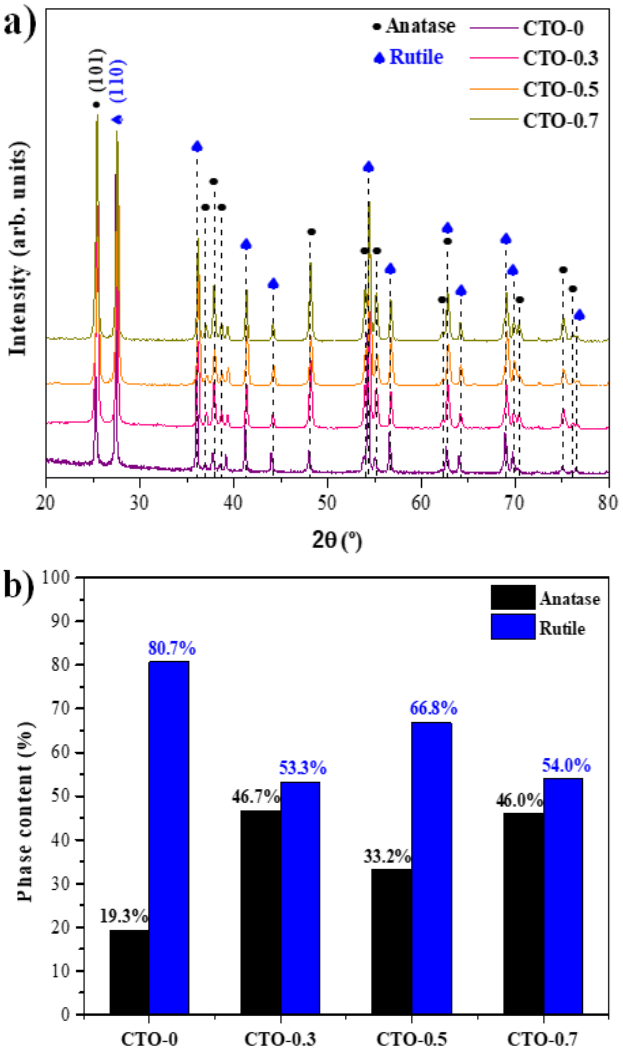

Figure 1. XRD patterns **(a)** and phase content **(b)** of CTO-0, CTO-0.3, CTO-0.5, and CTO-0.7 samples.

In order to quantify the proportions of anatase and rutile phases in the prepared samples, the Spurr and Myers (1957) method was employed, according to the Eq. 1, in which, f_a is the anatase percentage in sample, I_R and I_A are the integrated intensity of rutile (110) and anatase (101) peaks.

$$f_a = \frac{1}{\left(1 + 1.265\,\frac{I_R}{I_A}\right)} \quad (1)$$

The anatase and rutile crystallite sizes of all prepared samples were calculated according to the Scherrer's Eq. 2 (Alexander and Klug, 1950).

$$D = \frac{k\,\lambda}{\beta \cos\theta} \quad (2)$$

The k is a constant related to shape factor (about 0.9), λ is the X-ray wavelength of Cu Kα radiation

Eclética Química Journal, vol. 47, special issue 1, 2022, 130-140
ISSN: 1678-4618
DOI: 10.26850/1678-4618eqj.v47.1SI.2022.p130-140

(0.15406 nm), β is the full width at half maximum (FWHM) of the diffraction peak, and θ is the diffraction angle. The values of β and θ used were related to the predominant phase on sample, being the (101) and (110) crystal planes for anatase and rutile phases, respectively. The calculated anatase crystallite sizes were 37.0, 28.8, 23.7, and 27.6 nm for CTO-0, CTO-0.3, CTO-0.5, and CTO-0.7 samples, respectively. For rutile crystallite sizes, the obtained values were 42.3, 35.2, 25.3, and 33.7 nm for CTO-0, CTO-0.3, CTO-0.5, and CTO-0.7 samples, respectively.

It can be observed that the Cu insertion on the TiO_2 lattice promoted an anatase phase stabilization compared to the bare one, as can be seen by the higher weight fractions (Fig. 1b). The anatase to rutile phase transformation in TiO_2 is strongly dependent on the synthesis temperature and also on the intrinsic physicochemical properties and concentration of impurities on lattice (Choi *et al.*, 2010; Shannon and Pask, 1965). As already reported, Cu^{2+} ions are most probably located in interstitial positions into TiO_2 lattice on anatase phase and primarily on grain surface due to its relatively large difference in ionic radius related to Ti^{4+} ions, *i.e.*, 73 and 60.5 pm for Cu^{2+} and Ti^{4+} in octahedral sites. Besides that, the lower density and higher volume of unit cell of anatase compared to rutile phase also contribute for the Cu^{2+} interstitial occupation (Choi *et al.*, 2010; Gupta and Tripathi, 2011). The interstitial Cu^{2+} into TiO_2 lattice generates Ti–O–Cu bonds that led to an increase in strain energy necessary to anatase to rutile phase transformation, resulting in an inhibition of the grain growth (Choi *et al.*, 2010; Hanaor and Sorrell, 2011; Qi *et al.*, 2011; Shannon and Pask, 1965), as can be observed in the reduction of average crystallite size of anatase with increasing doping concentration. This strain energy needs to be overcome to the rearrangement of $[TiO_6]$ clusters, which have different spatial organizations in both phases. Once Cu^{2+} ions are located at interstitials positions, the energy required for rearrangement has increased due to its interactions with $[TiO_6]$ clusters.

Figure 2a shows the micro-Raman spectra for the Cu-doped and bare TiO_2 samples. Both anatase and rutile phase of TiO_2 exhibits characteristics Raman shift bands, being six vibrational modes Raman active for anatase and four for rutile phase. The characteristics Raman bands of anatase phase are approximately located at 144 cm^{-1} (E_g), 197 cm^{-1} (E_g), 399 cm^{-1} (B_{1g}), 513–519 cm^{-1} (overlap in Raman shifts values by two vibrational modes with symmetries A_{1g} e B_{1g}), and 639 cm^{-1} (E_g). For rutile phase, the Raman shifts bands are located at approximately 143 cm^{-1} (B_{1g}), 447 cm^{-1} (E_g), 612 cm^{-1} (A_{1g}), and 826 cm^{-1} (B_{2g}) (Naumenko *et al.*, 2012; Ohsaka *et al.*, 1978; Ricci *et al.*, 2013; Sahoo *et al.*, 2009). Another band nearly 238 cm^{-1} for rutile phase is characteristic of a second order scattering due to coupling of two optical phonons (Ohsaka *et al.*, 1978; Ricci *et al.*, 2013; Swamy and Muddle, 2006).

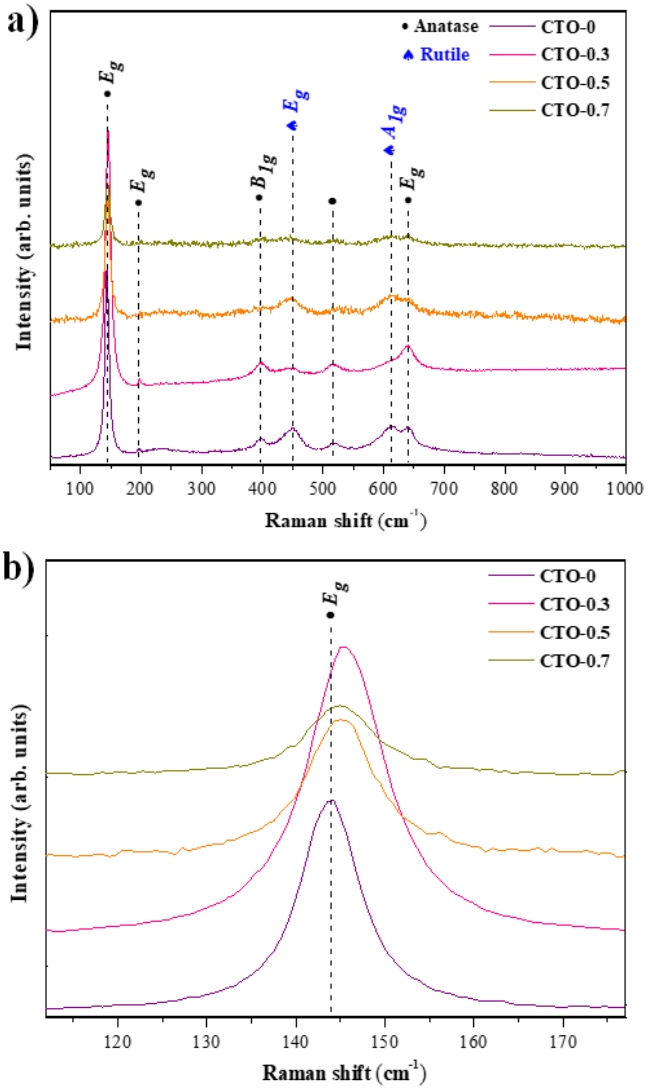

Figure 2. Raman spectra **(a)** and E_g Raman bands **(b)** of CTO-0, CTO-0.3, CTO-0.5, and CTO-0.7 samples.

It can be observed that the increase in Cu concentrations into TiO_2 induced a decrease in the intensities of Raman bands compared to the bare one. The structural Ti–O–Cu linkage formed by the interstitial Cu results in a hindrance of the $[TiO_6]$ clusters, reducing its freedom degree for the vibrational modes, hence decreasing the intensity of the Raman bands. Figure 1b shows the E_g Raman band position for the anatase phase for all prepared samples. It can be seen that the insertion of Cu into TiO_2 lattice induced a shift to higher frequencies, thus corroborating with the

Eclética Química Journal, vol. 47, special issue 1, 2022, 130-140
ISSN: 1678-4618
DOI: 10.26850/1678-4618eqj.v47.1SI.2022.p130-140

presence of Ti–O–Cu linkage that results in an increase in the strain energy.

Figure 2 shows the FE-SEM images of the Cu-doped and bare TiO_2 samples. It can be observed that all samples are composed of agglomerates of nanoparticles, which is characteristic of the Pechini method (Chen *et al.*, 2018b; Neris *et al.*, 2018). Furthermore, the agglomeration of these nanoparticles also arises from the annealing procedure, thus inducing their coalescence.

Photoluminescence spectroscopy emission measurements were performed to understand the effect of Cu insertion into TiO_2 structure in its optical behavior. Figure 3a shows the PL spectra of bare and Cu-doped TiO_2 samples. As can be seen, all spectra indicated the presence of two major emission bands, one located at 400–700 nm and the other centered at approximately 800 nm. The first one is characteristic of anatase phase emission and the second is characteristic of rutile phase emission, corroborating the XRD and Raman results (Jin *et al.*, 2015; Nasr *et al.*, 2015). The PL spectra for all prepared samples indicate a broadband profile, which is assigned to multiphonon processes. These processes arise from the presence of a high density of energy levels within the band gap, in which the electron momentum relaxation and hence photon emission occur in several pathways (Cruz *et al.*, 2020; Tello *et al.*, 2020). It can be seen that all Cu-doped samples presented a lower emission intensity compared to the bare one. This indicates a higher density of intermediate energy levels within the band gap for Cu-doped samples, which results in a lower recombination rate of the electron-hole pairs.

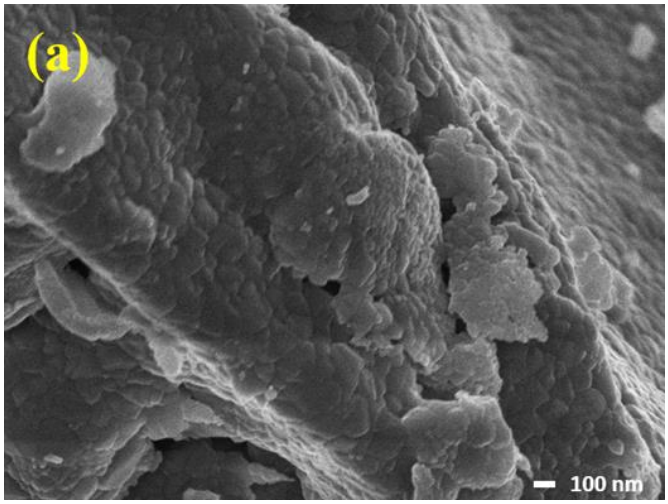

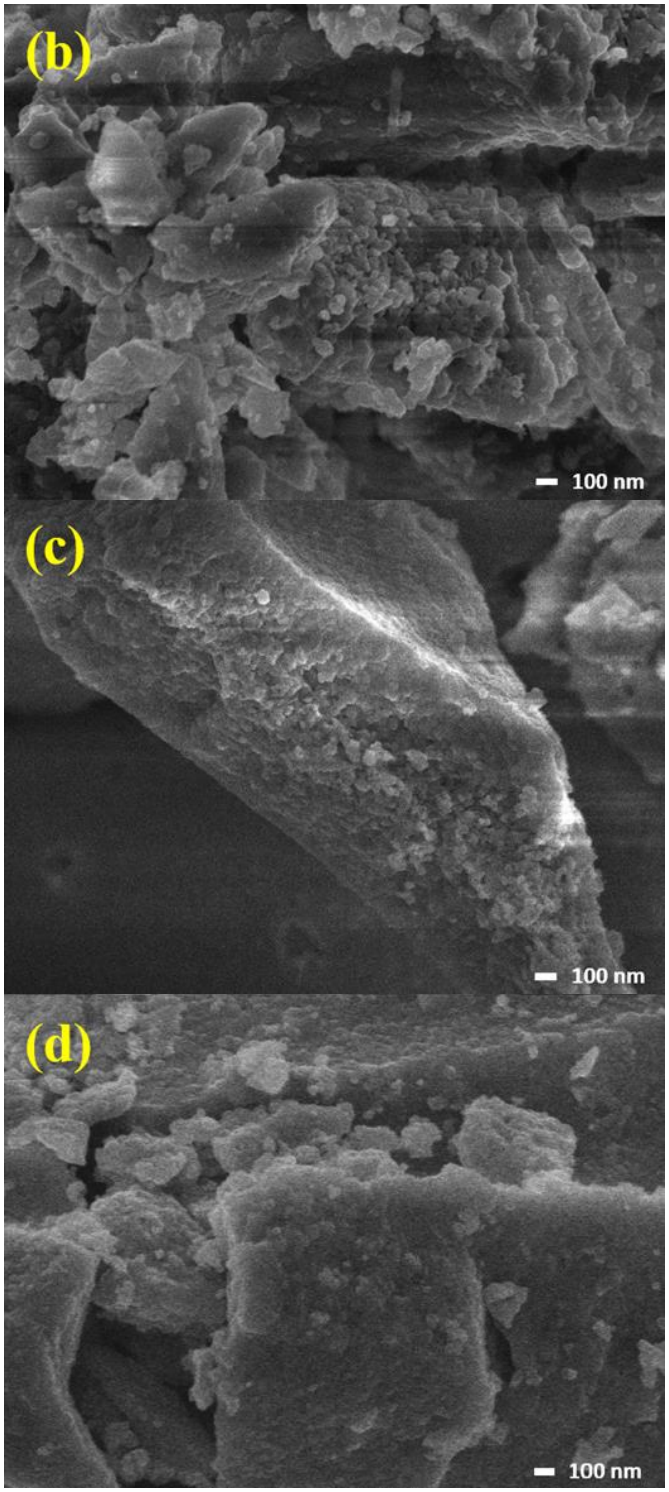

Figure 3. FE-SEM images of CTO-0 **(a)**, CTO-0.3 **(b)**, CTO-0.5 **(c)**, and CTO-0.7 **(d)** samples.

In order to investigate the contribution of defects for PL emissions in bare and Cu-doped TiO_2 samples, deconvolution of emission bands was performed using the PeakFit v.4 software. It is known that emissions in different color regions are due to different type of defects in the structure that contribute to the electronic

Eclética Química Journal, vol. 47, special issue 1, 2022, 130-140
ISSN: 1678-4618
DOI: 10.26850/1678-4618eqj.v47.1SI.2022.p130-140

transitions. The blue emissions have been associated with the structural distortions in the composing clusters of the lattice, whereas the green and yellow emissions have been associated with the oxygen vacancies (Longo *et al.*, 2008; Silva Junior *et al.*, 2015). As can be seen, the insertion of Cu into the TiO_2 lattice promoted a shift of the band emission for the blue region, as observed by the maximum emission wavelength and its percentage contribution in the Fig. 3b–e.

For clearer evidence, the contribution percentages of blue emission in function of the Cu-doping content are shown in Fig. 4f. It can be seen that the blue emission percentage directly increases with increasing Cu-doping content. Once the Cu^{2+} ions are occupying interstitial positions in the anatase phase of TiO_2, resulting in a Ti–O–Cu linkage, it is expected higher structural distortions in the [TiO_6] clusters compared to the bare one due to the atomic rearrangement. These structural distortions were confirmed by a higher contribution percentage of blue emission and corroborate the XRD and Raman results. Furthermore, the structural distortions in the [TiO_6] clusters caused by the Cu insertion into the TiO_2 lattice generate intermediate energy levels within the band gap, which decrease the recombination rate of electron-hole pairs and hence the PL emission intensity, as observed in Fig. 4a.

The photocatalytic activity of bare and Cu-doped TiO_2 samples was tested for RhB dye degradation under UV light irradiation. Figure 5a shows the RhB degradation percentage against the irradiation time for all prepared samples and the controlling test (photolysis).

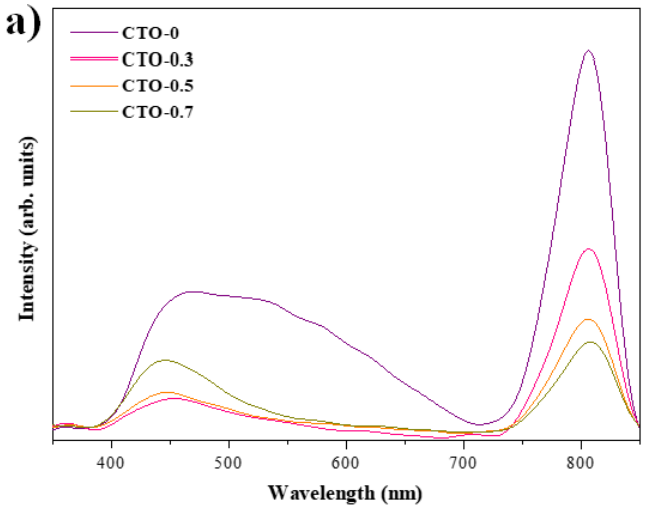

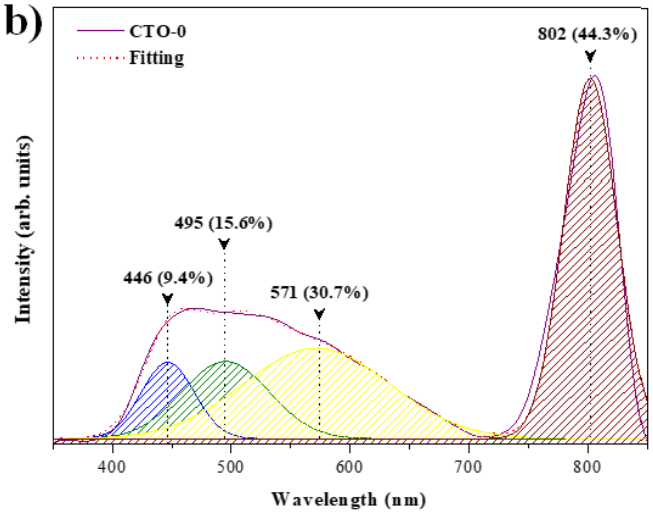

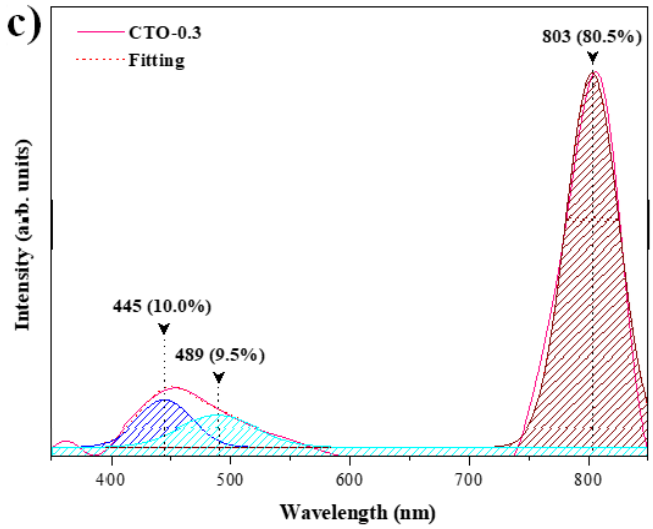

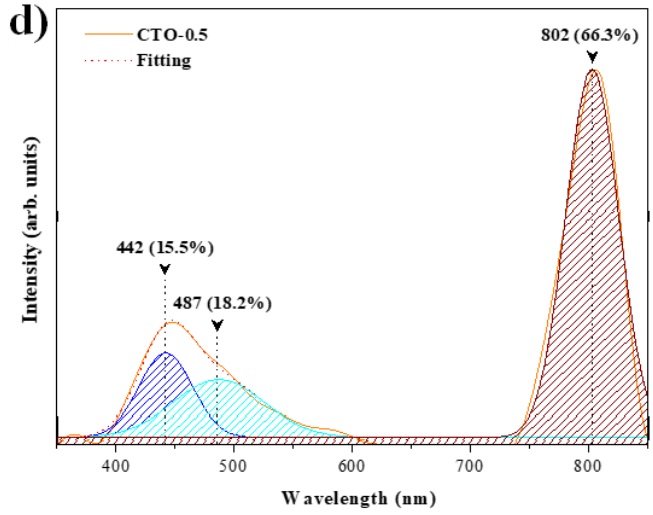

Eclética Química Journal, vol. 47, special issue 1, 2022, 130-140
ISSN: 1678-4618
DOI: 10.26850/1678-4618eqj.v47.1SI.2022.p130-140

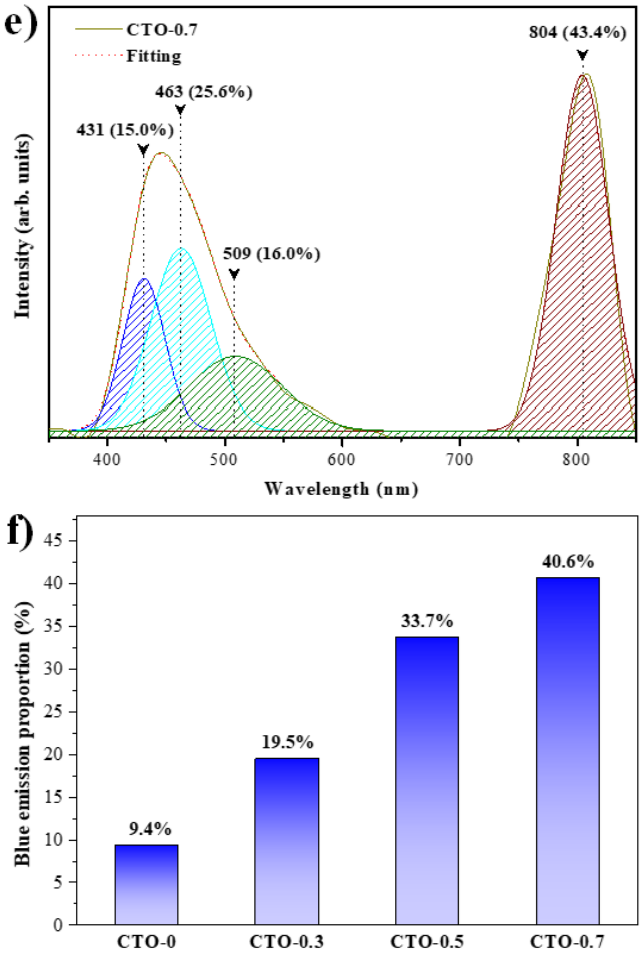

Figure 4. Photoluminescence spectroscopy spectra of all prepared samples **(a)**, deconvolution of emission band of CTO-0 **(b)**, CTO-0.3 **(c)**, CTO-0.5 **(d)**, and CTO-0.7 **(e)** samples, and blue emission percentage of all prepared samples **(f)**.

It was observed that all Cu-doped samples present a higher photocatalytic activity compared to the bare one. Further, the increase in the Cu-doping content led to an increase in the RhB degradation percentage in 90 min of reaction. However, the CTO-0.5 and CTO-0.7 samples presented similar photocatalytic activity, indicating a saturation of the Cu-content for the improvement of photocatalytic activity of the TiO_2. According to the Langmuir-Hinshelwood plot (Fig. 4b), the photocatalytic activity of all prepared samples presents a pseudo-first order kinetics (B. Liu *et al.*, 2014). The rate constants for those samples are depicted inset the Fig. 4b.

As previously mentioned, the Cu insertion into the TiO_2 lattice leads to the structural distortions in the $[TiO_6]$ clusters, which generate a higher density of intermediate energy levels within the band gap. These energy levels act as traps for the electronic transitions, thus decreasing the recombination rate of electron-hole pairs, as observed by PL analysis. Herewith, the decrease in the recombination rate leads to an increase in the lifetime of electron-hole pairs. Once these pairs have a higher lifetime, their availability to perform the redox reactions with the reaction medium are also increased. Therefore, the Cu insertion into the TiO_2 lattice caused structural distortions in the $[TiO_6]$ clusters that act as trap for electronic transitions, thus increasing the availability of electrons to promote the reduction reactions and holes to promote the oxidation reactions. These redox reactions rule the RhB degradation mechanism either by the generation of radical species that can degrade the RhB molecules as also by the direct degradation of RhB molecules adsorbed on the TiO_2 particle surface.

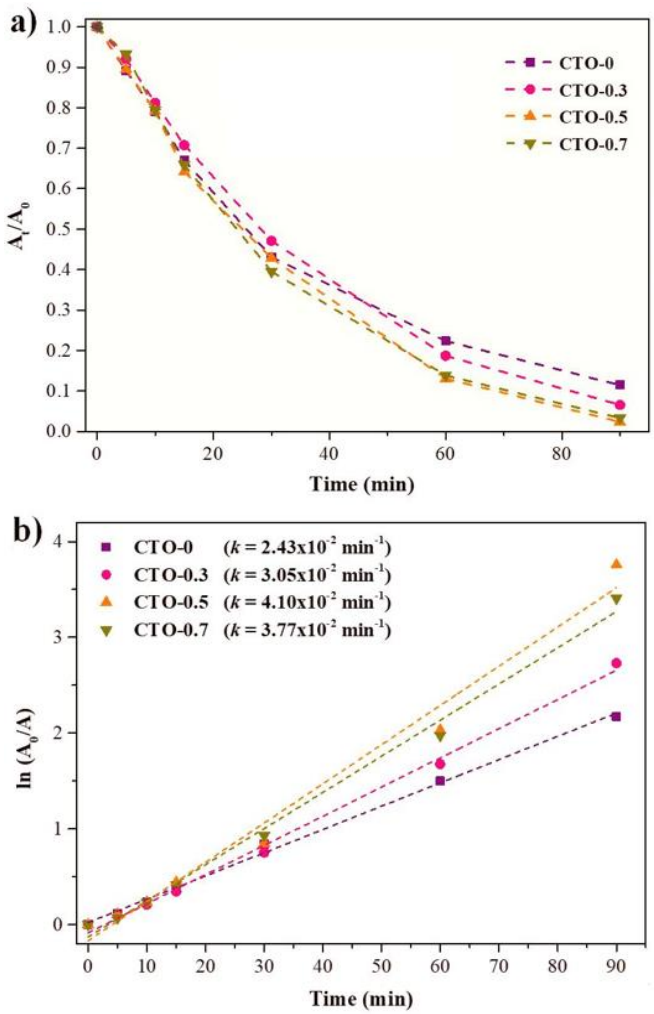

Figure 5. Relative absorbance of RhB dye solution against photocatalytic reaction time **(a)** and pseudo first-order kinetics plot **(b)** for CTO-0, CTO-0.3, CTO-0.5, and CTO-0.7 samples.

Eclética Química Journal, vol. 47, special issue 1, 2022, 130-140
ISSN: 1678-4618
DOI: 10.26850/1678-4618eqj.v47.1SI.2022.p130-140

The prepared CTO-0 sample has a composition very close to Degussa P25 (85% wt rutile and 15% wt anatase), one of the world's most used photocatalysts, but the photocatalytic active of this and of the all the CTOs obtained are small from the P25 activity. This was attributed to surface area difference since the P25 surface are 83 $m^2 g^{-1}$ and the obtained is a maximum of 15 $m^2 g^{-1}$) for CTO 0.5.

4. Conclusions

The Cu-doping into TiO_2 as powders samples were successfully obtained by the Pechini method. The insertion on Cu^{2+} into the TiO_2 structure promoted the anatase phase stabilization, increasing its content on the samples in relation to the pure TiO_2. This stabilization has been assigned to the interstitial occupation of Cu^{2+} in the anatase phase of TiO_2, thus increasing the strain energy required to the structural rearrangement for the transformation in rutile phase. The shift to higher vibrational frequencies in Raman analysis corroborated the occupation of Cu^{2+} in interstitial positions into TiO_2 structure. PL results indicated that the Cu-doping in TiO_2 induced structural distortions in $[TiO_6]$ clusters, which resulted in shift of PL emission band to blue region and a decrease in the PL emission intensity. The photocatalytic performance of TiO_2 samples under UV light irradiation were enhanced by the Cu-doping, which has been related to the formation of intermediate energy levels within band gap. These levels can act as electron trap, thus decreasing the recombination rate of electron-hole pairs and hence increasing their availability to perform the redox reactions with the reaction medium. Therefore, the Cu-doping into TiO_2 allowed structural and photocatalytic advantages in relation to the pure sample.

Authors' contribution

Conceptualization: Teodoro, V.; Perazolli, L. A.
Data curation: Teodoro, V.
Formal analysis: Teodoro, V.
Funding acquisition: Longo, E.; Zaghete, M. A.; Perazolli, L. A.
Investigation: Teodoro, V. Perazolli, L. A.
Methodology: Teodoro, V.
Project administration: Perazolli, L. A.
Resources: Longo, E.; Zaghete, M. A.; Perazolli, L. A.
Software: Not applicable.
Supervision: Longo, E.; Zaghete, M. A.; Perazolli, L. A.
Validation: Teodoro, V.
Visualization: Teodoro, V.; Longo, E.; Zaghete, M. A.; Perazolli, L. A.
Writing – original draft: Teodoro, V.
Writing – review & editing: Teodoro, V.; Longo, E.; Perazolli, L. A.

Data availability statement

All data sets were generated or analyzed in the current study.

Funding

Fundação de Amparo à Pesquisa do Estado de São Paulo (FAPESP). Grant No: 2013/07296-2.

Conselho Nacional de Desenvolvimento Científico e Tecnológico (CNPq). Grant No: 142035/2017-3.

Coordenação de Aperfeiçoamento de Pessoal de Nível Superior (CAPES). Finance Code: 001.

Acknowledgments

Not applicable.

References

Alexander, L.; Klug, H. P. Determination of crystallite size with the x-ray spectrometer. *J. Appl. Phys*. **1950**, *21* (2), 137–142. https://doi.org/10.1063/1.1699612

Carp, O.; Huisman, C. L.; Reller, A. Photoinduced reactivity of titanium dioxide. *Prog. Solid State Chem*. **2004**, *32* (1–2), 33–177. https://doi.org/10.1016/j.progsolidstchem.2004.08.001

Chen, W. F.; Chen, H.; Koshy, P.; Nakaruk, A.; Sorrell, C. C. Effect of doping on the properties and photocatalytic performance of titania thin films on glass substrates: Single-ion doping with Cobalt or Molybdenum. *Mater. Chem. Phys*. **2018a**, *205*, 334–346. https://doi.org/10.1016/j.matchemphys.2017.11.021

Chen, W. F.; Mofarah, S. S.; Hanaor, D. A. H.; Koshy, P.; Chen, H.-K.; Yue, J.; Sorrel, C. C. Enhancement of Ce/Cr codopant solubility and chemical homogeneity in TiO_2 nanoparticles through sol−gel versus Pechini syntheses. *Inorg. Chem*. **2018b**, *57* (12), 7279−7289. https://doi.org/10.1021/acs.inorgchem.8b00926

Choi, J.; Park, H.; Hoffmann, M. R. Effects of single metal-ion doping on the visible-light photoreactivity of TiO_2. *J. Phys. Chem. C*. **2010**, *114* (2), 783–792. https://doi.org/10.1021/jp908088x

Cruz, L.; Teixeira, M. M.; Teodoro, V.; Jacomaci, N.; Laier, L. O.; Assis, M.; Macedo, N. G.; Tello, A. C. M.; Silva, L. F.; Marques, G. E.; Zaghete, M. A.; Teodoro, M. D.; Longo, E. Multi-dimensional architecture of Ag/α-Ag_2WO_4 crystals: Insights into microstructural, morphological, and photoluminescence properties. *CrystEngComm*. **2020**, *22* (45), 7903–7917. https://doi.org/10.1039/D0CE00876A

Dashora, A.; Patel, N.; Kothari, D. C.; Ahuja, B. L.; Miotello, A. Formation of an intermediate band in the energy gap of TiO_2 by Cu – N-codoping : First principles study and experimental evidence. *Sol. Energy Mater. Sol. Cells*. **2014**, *125*, 120–126. https://doi.org/10.1016/j.solmat.2014.02.032

Fujishima, A.; Rao, T. N.; Tryk, D. A. Titanium dioxide photocatalysis. *J. Photochem. Photobiol. C Photochem. Rev*. **2000**, *1* (1), 1–21. https://doi.org/10.1016/S1389-5567(00)00002-2

Galindo, C.; Jacques, P.; Kalt A. Photodegradation of the aminoazobenzene acid orange 52 by three advanced oxidation processes : UV/H_2O_2 , UV/TiO_2 and VIS/TiO_2: Comparative mechanistic and kinetic investigations. *J. Photochem. Photobiol. A Chem*. **2000**, *130* (1), 35–47. https://doi.org/10.1016/S1010-6030(99)00199-9

Gaya, U. I.; Abdullah, A. H. Heterogeneous photocatalytic degradation of organic contaminants over titanium dioxide : A review of fundamentals , progress and problems. *J. Photochem. Photobiol. C Photochem. Rev*. **2008**, 9 (1), 1–12. https://doi.org/10.1016/j.jphotochemrev.2007.12.003

Gupta, S. M.; Tripathi, M. A review of TiO_2 nanoparticles. *Chin. Sci. Bull*. **2011**, *56*, 1639. https://doi.org/10.1007/s11434-011-4476-1

Hanaor, D. A. H.; Sorrell, C. C. Review of the anatase to rutile phase transformation. *J. Mater. Sci*. **2011**, *46*, 855–874. https://doi.org/10.1007/s10853-010-5113-0

Hu, Y.; Tsai, H.-L.; Huang, C.-L. Phase transformation of precipitated TiO_2 nanoparticles. *Mater. Sci. Eng. A* **2003**, *344* (1–2), 209–214. https://doi.org/10.1016/S0921-5093(02)00408-2

Jin, C.; Liu, B.; Lei, Z.; Sun, J. Structure and photoluminescence of the TiO_2 films grown by atomic layer deposition using tetrakis-dimethylamino titanium and ozone. *Nanoscale Res. Lett*. **2015**, 10, 95–103. https://doi.org/10.1186/s11671-015-0790-x

Li, J.; Xu, X.; Liu, X.; Yu, C.; Yan, D.; Sun, Z.; Pan, L. Sn doped TiO_2 nanotube with oxygen vacancy for highly efficient visible light photocatalysis. *J. Alloys Compd*. **2016**, *679*, 454–462. https://doi.org/10.1016/j.jallcom.2016.04.080

Liu, B.; Zhao, X.; Terashima, C.; Fujishima, A.; Nakata. K. Thermodynamic and kinetic analysis of heterogeneous photocatalysis for semiconductor systems. *Phys. Chem. Chem. Phys*. **2014**, *16* (19), 8751–8760. https://doi.org/10.1039/c3cp55317e

Liu, G.; Wang, L.; Yang, H. G.; Cheng, H. M.; Lu, G. Q. Titania-based photocatalysts—crystal growth, doping and heterostructuring. *J. Mater. Chem*. **2010**, *20* (5), 831–843. https://doi.org/10.1039/B909930A

Longo, V. M.; Figueiredo, A. T.; Lázaro S.; Gurgel, M. F.; Costa, M. G. S.; Paiva-Santos, C. O.; Varela, J. A.; Longo, E.; Masteralo, V. R.; De Vicente, F. S.; Hernandes, A. C.; Franco, R. W. A. Structural conditions that leads to photoluminescence emission in $SrTiO_3$: An experimental and theoretical approach. *J. Appl. Phys*. **2008**, *104* (2), 023515. https://doi.org/10.1063/1.2956741

Nakata, K.; Fujishima, A. TiO_2 photocatalysis : Design and applications. *J. Photochem. Photobiol. C Photochem. Rev*. **2012**, *13* (3), 169–189. https://doi.org/10.1016/j.jphotochemrev.2012.06.001

Nasr, M.; Chaaya, A. A.; Abboud, N.; Bachelany, M.; Viter, R.; Eid, C.; Khoury, A.; Miele, P. Photoluminescence: A very sensitive tool to detect the presence of anatase in rutile phase electrospun TiO_2 nanofibers. *Superlattices Microstruct*. **2015**, *77*, 18–24. https://doi.org/10.1016/j.spmi.2014.10.034

Naumenko, A.; Gnatiuk, I.; Smirnova, N.; Eremenko, A. Characterization of sol-gel derived TiO_2/ZrO_2 films and powders by Raman spectroscopy. *Thin Solid Films*. **2012**, *520* (14), 4541–4546. https://doi.org/10.1016/j.tsf.2011.10.189

Neris, A. M.; Schreiner, W. H.; Salvador, C.; Silva, U. C.; Chesman, C.; Longo, E.; Santos, I. M. G. Photocatalytic evaluation of the magnetic core@shell system (Co,Mn)Fe_2O_4@TiO_2 obtained by the modified

Pechini method. *Mater. Sci. Eng. B*. **2018**, *229*, 218–226. https://doi.org/10.1016/j.mseb.2017.12.029

Ohsaka, T.; Izumi, F.; Fujiki, Y. Raman spectrum of anatase, TiO_2. *J. Raman Spectrosc*. **1978**, *7* (6), 321–324.

Qi, F.; Moiseev, A.; Deubener, J.; Weber, A. Thermostable photocatalytically active TiO_2 anatase nanoparticles. *J. Nanoparticle Res*. **2011**, 13, 1325–1334. https://doi.org/10.1007/s11051-010-0211-0

Qourzal, S.; Tamimi, M.; Assabbane, A.; Ait-Ichou, Y. Photocatalytic degradation and adsorption of 2-naphthol on suspended TiO_2 surface in a dynamic reactor. *J. Colloid Interface Sci*. **2005**, *286* (2), 621–626. https://doi.org/10.1016/j.jcis.2005.01.046

Rashad, M. M.; Ismail, A. A.; Osama, I.; Ibrahim, I. A.; Kandil, A.-H. T. Photocatalytic decomposition of dyes using ZnO doped SnO_2 nanoparticles prepared by solvothermal method. *Arab. J. Chem*. **2014**, *7* (1), 71–77. https://doi.org/10.1016/j.arabjc.2013.08.016

Ricci, P. C.; Carbonaro, C. M.; Stagi, L.; Salis, M.; Casu, A.; Enzo, S.; Delogu, F. Anatase-to-rutile phase transition in TiO_2 nanoparticles irradiated by visible light. *J. Phys. Chem. C* **2013**, *117* (15), 7850–7857. https://doi.org/10.1021/jp312325h

Sahoo, S.; Arora, A. K.; Sridharan, V. Raman line shapes of optical phonons of different symmetries in anatase TiO_2 nanocrystals. *J. Phys. Chem. C*. **2009**, *113* (39), 16927–16933. https://doi.org/10.1021/jp9046193

Sanchez-Dominguez, M.; Morales-Mendoza, G.; Rodriguez-Vargas, M. J.; Ibarra-Malo, C. C.; Rodriguez-Ridriguez, A. A.; Vela-Gonzalez, A. V.; Perez-Garcia, S. A.; Gomez, R. Synthesis of Zn-doped TiO_2 nanoparticles by the novel oil-in-water (O/W) microemulsion method and their use for the photocatalytic degradation of phenol. *J. Environ. Chem. Eng*. **2015**, *3* (4) (Part B), 3037–3047. https://doi.org/10.1016/j.jece.2015.03.010

Shannon, R. D.; Pask, J. A. Kinetics of the anatase-rutile transformation. *J. Am. Ceram. Soc*. **1965**, *48* (8), 391–398. https://doi.org/10.1111/j.1151-2916.1965.tb14774.x

Silva Junior, E; La Porta, F. A.; Liu, M. S.; Andrés, J.; Varela, J. A.; Longo, E. A relationship between structural and electronic order–disorder effects and optical properties in crystalline TiO_2 nanomaterials. *Dalt. Trans*. **2015**, *44* (7), 3159–3175. https://doi.org/10.1039/C4DT03254C

Silva, J. S.; Machado, T. R.; Trench, A. B.; Silva, A. D.; Teodoro, V.; Vieira, P. C.; Martins, T. A.; Longo, E. Enhanced photocatalytic and antifungal activity of hydroxyapatite/α-$AgVO_3$ composites. *Mater. Chem. Phys*. **2020**, *252*, 123294. https://doi.org/10.1016/j.matchemphys.2020.123294

Spurr, R. A.; Myers, H. Quantitative analysis of anatase-rutile mixtures with an x-ray diffractometer. *Anal. Chem*. **1957**, *29* (5), 760–762. https://doi.org/10.1021/ac60125a006

Swamy, V.; Muddle, B. C. Size-dependent modifications of the Raman spectrum of rutile TiO_2. *Appl. Phys. Lett*. **2006**, *89*, 163118. https://doi.org/10.1063/1.2364123

Tello, A. C. M.; Assis, M.; Menasce, R.; Gouveia, A. F.; Teodoro, V.; Jacomaci, N.; Zaghete, M. A.; Andrés, J.; Marques, G. E.; Teodoro, M. D.; Silva, A. B. F.; Bettini, J.; Longo, E. Microwave-driven hexagonal-to-monoclinic transition in $BiPO_4$: An in-depth experimental investigation and first-principles study. *Inorg Chem*. **2020**, *59* (11), 7453–7468. https://doi.org/10.1021/acs.inorgchem.0c00181

Vargas Hernández, J.; Coste, S.; García Murillo, A.; Carrillo Romo, F.; Kassiba, A. Effects of metal doping (Cu, Ag, Eu) on the electronic and optical behavior of nanostructured TiO_2. *J. Alloys Compd*. **2017**, *710*, 355–363. https://doi.org/10.1016/j.jallcom.2017.03.275

Wang, H.; Li, Y.; Ba, X.; Huang, L.; Yu, Y. TiO_2 thin films with rutile phase prepared by DC magnetron co-sputtering at room temperature: Effect of Cu incorporation. *Appl. Surf. Sci*. **2015**, 345, 49–56. https://doi.org/10.1016/j.apsusc.2015.03.106

Wang, Q.; Jin, R.; Zhang, M.; Gao, S. Solvothermal preparation of Fe-doped TiO_2 nanotube arrays for enhancement in visible light induced photoelectrochemical performance. *J. Alloys Compd*. **2017**, *690*, 139–144. https://doi.org/10.1016/j.jallcom.2016.07.281

Wang, S.; Meng, K. K.; Zhao, L.; Jiang, Q.; Lian, J. S. Superhydrophilic Cu-doped TiO_2 thin film for solar-driven photocatalysis. *Ceram. Int*. **2014**, *40* (4), 5107–5110. https://doi.org/10.1016/j.ceramint.2013.09.028

Eclética Química Journal, vol. 47, special issue 1, 2022, 130-140
ISSN: 1678-4618
DOI: 10.26850/1678-4618eqj.v47.1SI.2022.p130-140

Xiao, J.; Xie, Y.; Cao, H.; Nawaz, F.; Zhang, S.; Wang, Y. Disparate roles of doped metal ions in promoting surface oxidation of TiO_2 photocatalysis. *J. Photochem. Photobiol. A Chem*. **2016**, *315*, 59–66. https://doi.org/10.1016/j.jphotochem.2015.09.013

Zhang, L.; Guo, J.; Huang, X.; Zhang, Y.; Han, Y. The dual function of Cu-doped TiO_2 coatings on titanium for application in percutaneous implants. *J. Mater. Chem. B* **2016**, *4* (21), 3788–3800. https://doi.org/10.1039/C6TB00563B

Zhang, L.; Li, Y.; Zhang, Q.; Wang, H. Well-dispersed Pt nanocrystals on the heterostructured TiO_2/SnO_2 nanofibers and the enhanced photocatalytic properties. *Appl. Surf. Sci*. **2014**, *319*, 21–28. https://doi.org/10.1016/j.apsusc.2014.07.199

Zhang, Y.; Meng, Y.; Zhu, K.; Qiu, H.; Ju, Y.; Gao, Y.; Du, F.; Zou, B.; Chen, G.; Wei, Y. Copper-doped titanium dioxide bronze nanowires with superior high rate capability for lithium ion batteries. *Appl. Mater. Interfaces* **2016**, *8* (12), 7957–7965. https://doi.org/10.1021/acsami.5b10766

Zhu, S.-C.; Xie, S.-H.; Liu, Z-P. Nature of rutile nuclei in anatase-to-rutile phase transition. *J. Am. Chem. Soc*. **2015**, *137* (35),11532–11539. https://doi.org/10.1021/jacs.5b07734

ISSN: 1678-4618
DOI: 10.26850/1678-4618eqj.v47.1SI.2022.p130-140